RGNZ/MGPB

Rudarsko-geološko-naftni zbornik
(The Mining-Geology-Petroleum Engineering Bulletin)
DOI: 10.17794/rgn.2026.3.2

Original scientific paper

Integrated Mathematical and Physical Modelling of Salt Ions Leaching from Coal-Mining Waste: Implications for Ecological Safety and Civil Protection

Vasyl Karabyn[1]*, Iryna Kochmar[2], Oksana Karabyn[3], Clint Sutherland[4], Valentyna Loboichenko[5,6], Andrii Khorolskyi[7]

[1] *Department of Civil Protection, Lviv State University of Life Safety, Lviv, Ukraine.*
[2] *Department of Environmental Safety, Lviv State University of Life Safety, Lviv, Ukraine.*
[3] *Department of Applied Mathematics and Mechanics, Lviv State University of Life Safety, Lviv, Ukraine.*
[4] *Project Management and Civil Infrastructure Systems, The University of Trinidad and Tobago, Trinidad.*
[5] *Departamento de Ingeniería Energética, Escuela Técnica Superior de Ingeniería, Universidad de Sevilla, Camino de los Descubrimientos s/n., Sevilla, Spain.*
[6] *Department of Civil Security, Lutsk National Technical University, Lvivska St., 75, Lutsk, Ukraine.*
[7] *Laboratory of Mining Problems, Branch for Physics of Mining Processes of the National Academy of Sciences of Ukraine, Dnipro, Ukraine.*

Abstract

Coal-mining waste heaps represent a significant source of dissolved salts that can be mobilised by precipitation, posing risks to ecological safety and civil protection. This study focuses on the Chervonohrad Central Concentration Plant spoil heap in western Ukraine, where both thermally altered and unaltered argillite were tested. Laboratory column experiments were performed on 100 g samples flushed with deionised water to simulate leaching under controlled conditions. The cumulative leachate volumes reached approximately 432 L, allowing quantification of total dissolved solids and ion-specific contributions. We flushed 100 g columns for 24 h at 300 mL·min^{-1} (8.5 L recirculated; ≈ 432 L passed), which yielded final filtrate total dissolved solids of 462 vs. 185 mg·L^{-1} for burnt and unburnt argillite and cumulative leached masses of 3.93 vs. 1.57 g (≈ 2.5× higher for burnt). Early-time contrast was also strong: after 2 h (≈ 0.7 L), burnt reached 183 mg·L^{-1} vs. 50 mg·L^{-1} (≈3.7×). Physical observations were combined with a mathematical modelling approach to establish a precipitation-response relationship linking annual rainfall to total dissolved solids release. The results indicate a strong linear increase of annual salt release with precipitation, with burnt materials exhibiting markedly higher fluxes. This integrated framework demonstrates how laboratory data and simple models can be applied to anticipate pollutant releases, supporting ecological safety and informing civil protection measures in coal-mining regions prone to hydrological extremes.

Keywords:
civil protection, ecological safety, emergency warning, geochemistry, predictive modelling

1. Introduction

Coal-fired power generation reached a new high of 10.7 TW h in 2024, primarily driven by electricity demand, which consumes roughly two-thirds of global coal and supplies about 35% of the world's electricity. In Ukraine, coal reserves exceed 117 Gt, representing over 90% of the country's fossil fuel resources, thus critically underpinning the national energy infrastructure (**International Energy Agency, 2025**). Expansive coal waste piles throughout Europe, including those in Ukraine, represent significant environmental challenges resulting from decades of coal mining and beneficiation activities. These wastes contain a heterogeneous mixture of minerals, including sulphide phases such as pyrite (FeS_2) and chalcopyrite ($FeCuS_2$), together with carbonates, silicates and halite-type salts. As water and oxygen infiltrate the waste material, these minerals undergo oxidation and dissolution, releasing a wide range of major ions, such as SO_4^{2-}, HCO_3^-, Cl^-, Na^+, K^+, Ca^{2+}, and Mg^{2+}, into surrounding waters. For example, pyrite oxidation generates sulphate and acidity, which in turn enhance the release of major cations and trace metals. This acidification promotes the mobility of toxic elements including Zn, Pb, Mn, Cu, and Fe, thereby increasing the risk of groundwater and surface water contamination (**Kochmar and Karabyn, 2023; Rouhani et al., 2023; Rouhani et al., 2024**). Microbial redox transformations are a primary control on leachate chemistry in mine-waste settings. Experiments with *Desulfuromonas* sp. have shown that bacteria can reduce sulfate/sulfur and alter

* Corresponding author: Vasyl Karabyn
e-mail address: vasyl.karabyn@gmail.com
Received: 6 September 2025. Accepted: 14 November 2025.
Available online: 14 May 2026

oxidized nitrogen species under iron-mediated conditions - processes mechanistically aligned with redox pathways expected in spoil-leachate systems (**Moroz et al., 2020**). Studies highlight that biosorption techniques (**Sutherland et al., 2023**) and biomodification of waste rock with sulfate-reducing bacteria are promising methods for the treatment of mine wastewater from sulfur and heavy metals (**Xu et al., 2025**). Studies highlight that biosorption techniques are promising for the remediation of heavy metals in such systems; however, their large-scale implementation remains technically challenging (**Sutherland et al., 2023**). Future investigations may also benefit from incorporating machine learning models to improve spatial prediction accuracy for heavy metal distributions in mining-affected soils (**Proshad et al., 2025**).

The environmental and human health impacts of elevated concentrations of major anions such as SO_4^{2-}, Cl^-, and HCO_3^- are profound. These impacts include increased risks of groundwater contamination, degradation of water bodies, and associated public health hazards, notably heavy metal exposure and fluorosis (**Loboichenko and Leonova, 2021; Xu et al., 2024; Tkachenko et al., 2021**). Uncontrolled disposal of waste rock by introducing it into the soil, including for agricultural purposes, changes its pH and negatively affects the qualitative and quantitative composition of the microbiome. Accordingly, this may have consequences for the food security of the state (**Garbacz at al., 2025**). Moreover, coal waste sites significantly heighten the risk of environmental emergencies such as spontaneous combustion, landslides, and acute contamination events (**Hoxha et al., 2025; Petlovanyi et al., 2023; Monteiro et al., 2025**). However, even after the closure of coal mines and the implementation of reclamation measures, excess polutant are observed in water bodies located downstream of these mines. (**Cooke et al., 2025**). Due to the seepage of sediments, leaching of pollutants occurs along with further entry into natural ecosystems. Negative cumulative effects may occur due to the additional impact of mine waters, in the presence of several mining centers (**Tyndyk et al., 2024**).

These environmental emergencies pose severe challenges to civil protection systems, particularly in Ukraine. The State Emergency Service must coordinate responses across mining regions whereas managing limited resources during wartime conditions. Recent technological advancements, such as ground robot technologies, provide new avenues for monitoring and mitigating these risks, especially under hazardous conditions typical of post-mining landscapes (**Gromek and Lowe, 2025**). Given these risks, it is crucial to quantify the leaching of major ions under realistic precipitation conditions, as their concentrations, especially sulphates, chlorides, and bicarbonates, directly affect pH and metal transport. This study combines column experiments with a linear model to quantify total dissolved solids (TDS) leaching from the waste dump of a coal enrichment plant. Current precipitation-driven TDS models lack integration with civil protection frameworks, limiting their utility for emergency preparedness and community risk assessment in coal mining regions. While many studies characterise TDS leaching and management, comparatively few develop precipitation-driven annual-load models for coal-mine spoils; recent syntheses and related leaching work underscore this gap (**Welch et al., 2021; Daniels et al., 2016b; Castillo-Meza et al., 2020; Gao et al., 2025**). The predictive models developed estimate annual sulfur mobilisation, particularly emphasising climatic factors like precipitation. Comparative analyses illustrate how climate and geology modulate acid mine drainage (AMD) severity, as humid climates sustain continuous leaching, whereas arid regions experience episodic pulses (**Alvarenga et al., 2021; Rouhani et al., 2024**).

This research addresses a crucial gap by modelling the mobilisation of major ions from coal waste materials at the Chervonohrad Central Concentration Plant (CCCP) waste pile, emphasising the ecological impacts of sulphide mineral oxidation and the consequent potential for environmental emergencies. The integrated methodological approach informs risk assessment and environmental management tailored to Ukraine's temperate climatic conditions, while also providing a transferable framework for other mining regions and supporting the development of integrated environmental - civil protection response systems. Understanding the leaching behaviour of sulphate-rich mine wastes is essential not only for hydrogeochemical modelling but also for assessing risks to civil protection and emergency response planning in mining regions. Embedding such predictive frameworks within broader strategic environmental assessment instruments would further enhance their utility for civil protection and sustainable resource management (**Karabyn et al., 2022**). The study area and the laboratory methods underpin the model calibration and scaling.

2. Materials and methods

2.1. Study Area

The CCCP, operational since 1979 in Ukraine's Lviv-Volyn coal basin, has served as a key facility for processing low-grade coal from surrounding mines. The substantial waste pile at CCCP covers approximately 0.8638 km² and rises to 68 m, encompassing about 48.89 Mm³ of waste at an average density of 2680 kg·m^{-3} (**Bosak et al., 2020**). The accumulated waste poses environmental risks because of its large volume and the possibility of pollutant leaching. The study area is in Western Polissya, a humid continental (Dfb) climate zone with cold winters and warm summers. Meteorological data from the Volodymyr weather station indicate significant an-

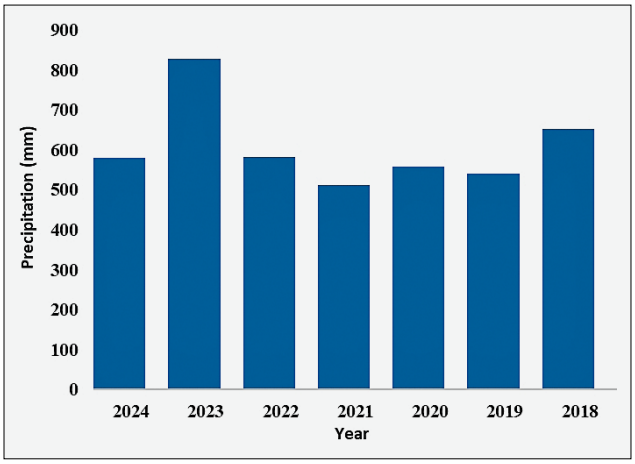

Figure 1. Total annual rainfall observed at Volodymyr station (Ukraine) during 2018-2024 (**URL 1**).

nual precipitation variability of 511 - 829 mm (see **Figure 1**), which provides the range used later for precipitation-based projections.

The CCCP waste primarily consists of argillite, siltstone, sandstone, and coal-associated sediments. The predominant minerals-siderite ($FeCO_3$), pyrite (FeS_2), and chalcopyrite ($FeCuS_2$) - undergo oxidation, significantly contributing to environmental contamination through iron and sulphur mobilisation (**Kochmar et al., 2024**). As a consequence, these mineralogical processes promote the leaching of major ions and trace metals into surrounding hydrological systems (**Karabyn and Kochmar, 2025**). Leachate from the site may reach nearby surface waters such as the Western Bug River, which flows into the Vistula. As Vistula runs mostly through Poland, this transboundary connection requires coordinated monitoring and management.

Documented landslides, groundwater contamination, and episodes of spontaneous combustion in waste piles underscore the need for robust hazard-mitigation measures to protect regional ecosystems and communities (**Kochmar et al., 2022; Petlovanyi et al., 2023**). Understanding precipitation-driven leaching processes is essential for designing targeted environmental protection measures, improving waste management practices in Ukraine's coal basin.

2.2. Research methods

Column experiments and processing of results. To simulate the leaching dynamics of TDS from spoil rock, a laboratory-scale column experiment was conducted using an apparatus assembled at the Environmental Safety Laboratory, Lviv State University of Life Safety (**Kochmar et al., 2024; Stepova et al., 2023**). The test material was argillite collected from the CCCP spoil heap. Ten grab samples from different sectors of the heap were composited to improve spatial coverage, then air-dried at 20-25°C to constant mass over 30 d, gently comminuted in an agate mortar, and dry-sieved through a 1.25 mm stainless-steel mesh. The < 1.25 mm fraction was used in subsequent leaching tests, with no secondary fractionation. Sampling targeted 0.2-0.3 m to capture the biologically active and hydrologically responsive near-surface layer of the spoil, where infiltration, oxygen exchange, and temperature fluctuations are most pronounced, promoting sulphide oxidation, dissolution of readily soluble salts, and mobilisation of sulphate and chloride ions. A similar focus on near-surface layers has been used for coal-waste piles undergoing self-heating, where the upper horizons control infiltration and thereby increase the leaching of major ions and potentially toxic elements (**Espinha Marques et al., 2024, Anghelescu and Diaconu, 2024**).

For the tests, two material conditions were used: unburned argillite; and thermally altered argillite obtained by laboratory firing of the composite material in a muffle furnace for 4 h at temperatures up to 600°C. In this study, "thermally altered (burnt) argillite" refers to argillite that has undergone oxidation and partial mineralogical transformation through laboratory firing at 600°C, producing a reddish-brown material. The term "unaltered (unburnt) argillite" denotes material that has not experienced thermal alteration and retains the original grey, compact lithology typical of the parent rock. Each experiment used a 100 g subsample packed into a vertical column 10 cm high and 36 mm in diameter (cross-sectional area 0.001018 m^2; packed volume ≈101.8 cm^3) (see **Figure 2**). To ensure reliability, each treatment was run in triplicate: three identical columns were packed in parallel with the same mass of material (burnt or unburnt) and operated under identical flow and temperature conditions. Leachate was collected from each column at corresponding time intervals and analysed separately for TDS; reported values are means across the three parallel runs, which were used for the precipitation-response modelling. The corresponding standard deviations did not exceed the instrument's measurement accuracy.

The concentrations of major ions in the filtrate were determined using standard chemical analysis methods at the Environmental Safety Laboratory at Lviv State University of Life Safety (certificate of attestation No. RL 091/21, dated 11/30/2021). In particular, acid titration to the appropriate end-point pH following Standard Methods was used (HCO_3^-); argentometric titration with silver nitrate and potassium chromate as indicator, according to the Mohr method, was applied (Cl^-). EDTA complexometric titration with murexide and Eriochrome Black T was performed (Ca^{2+} and Mg^{2+}), with magnesium calculated by difference. Gravimetric determination as barium sulphate after precipitation with Ba^{2+} and subsequent ignition and drying of the $BaSO_4$ precipitate was used (SO_4^{2-}). Sodium and potassium (Na^+, K^+) were estimated by the ionic charge balance method, based on equivalents of the directly determined major ions (**APHA, 2017**).

The leaching system comprised a vertical filtration column and a circulation pump that continuously drove

Figure 2. Laboratory setup showing the column apparatus used for TDS leaching experiments.

deionized water through the packed bed. Deionized water (8.5 L) was recirculated at 300 mL·min⁻¹ for 24 h, yielding a cumulative passed volume of ≈432 L (≈50 flushing cycles). Aliquots of the filtrate were collected at fixed intervals (every 4 h over 24 h), with additional early-time sampling during the first 2 h of circulation (**Kochmar et al., 2024**).

Filtrate samples were collected at multiple time intervals and analysed for TDS (mg·L⁻¹), which were derived from measurements of electrical conductivity (EC). EC was measured with a bench-top EC 215 (Hanna Instruments), which automatically converts EC to TDS using a built-in conversion factor. The meter was two-point calibrated daily with standards bracketing the sample range and verified against a mid-range check, with recalibration performed if drift exceeded ±2%. The manufacturer-stated accuracy is ±1% of full scale. TDS values were calculated from temperature-corrected EC at 25°C according to the relationship TDS = $f \times EC_{25}$, with $f = 0.50$ appropriate for sulphate-rich matrices. The method detection limit was 1.5 mg·L⁻¹ (based on 3σ of low-level EC checks at 25°C, converted to TDS). Quality control included reagent blanks, duplicate aliquots (~10%), and periodic check-standards (every 2 h), all within predefined acceptance limits.

Concentrations were multiplied by the cumulative filtrate volume to calculate cumulative mass (M) at each sampling stage; dividing M by the passed volume V yielded the mean leachate concentration (mg·L⁻¹). The results were used to model both the cumulative leaching behaviour and the incremental leachate concentration per unit water volume. The latter was obtained by calculating the change in TDS-derived mass over the change in water volume between successive sampling points, providing a dynamic view of concentration evolution throughout the experiment. Based on the observed ***M-V*** relationship, a linear regression model was fitted to describe salt removal as a function of water input. The model estimated $M = a_v \cdot V + b_v$, where M is cumulative leached mass and V is passed water volume. The regression coefficients a_v (mg·L⁻¹) and b_v (mg) were derived from experimental data and subsequently used to parameterise the site-scale precipitation model.

A two-stage approach was applied to process the column data. The primary experimental values were the TDS (mg·L⁻¹) in the leachate measured at specific time intervals. At the first stage, these values were converted into the cumulative mass of leached salts M (mg) by volume-weighting across successive sampling intervals:

$$M_i = \Delta V_i \sum_j TDS_j \quad (1)$$

where ΔV_i is the incremental water volume between samplings.

At the second stage, the **incremental leachate concentration** between successive points was computed as:

$$\left(\frac{dM}{dV}\right)_i \approx \frac{M_i - M_{i-1}}{V_i - V_{i-1}}, \text{(mg·L}^{-1}\text{)} \quad (2)$$

Calibration of column-derived regression coefficients for model parametrisation. Column data were used **solely to calibrate** the linear mass-volume relation $M=a_vV+b_v$ for each material (burnt vs unburnt), yielding a_v (mg·L⁻¹) and b_v (mg). These **dimensional** coefficients are then **transferred to the site scale** in the mathematical model, where the real spoil area S_{site}, spoil mass $m_{ore,site}$, hydrologic partitioning ($V_{p,site}$, $V_{f,site}$) and annual duration T=1 yr govern the predicted mass export as a function of precipitation. To avoid ambiguity with the **dimensionless** formulation used later, we denote the column-regression coefficients by a_v, b_v here; when introduced into the site-scale dimensionless expression, they appear through **dimensionless combinations** denoted as a, b.

Column data were used **solely to calibrate** the linear mass-volume relation $M=aV+b$ for each material (burnt vs unburnt), yielding the regression coefficients a_v (mg·L⁻¹) and b_v (mg). These coefficients are then **transferred to the site scale** in the mathematical model, where the **real spoil area** S_{site}, **spoil mass** $m_{ore,\,site}$ **hydrologic partitioning** ($V_{p,\,site,}$ $V_{f,\,site}$) and **annual duration** T=1 yr govern the predicted mass export as a function of precipitation. Thus, while the column analysis is expressed in terms of cumulative water throughput (M, V), the **field application** uses the calibrated (a, b) with **site-specific geometry and hydroclimate**.

Statistical processing of column data. For each treatment (unburnt and burnt), the cumulative mass–volume relation was fitted by ordinary least squares (OLS) as $M = a_vV + b_v$. We report the slope a_v, intercept b_v, their standard errors (SE_a, SE_b), the coefficient of determina-

tion (R^2) and the sample size (n). Two-sided 95% confidence intervals (CI) for the slope were computed as $a_v \pm t_{0.975,n-2}\, SE_a$, where $t_{0.975,n-2}$ is the Student's t-critical value for $n-2$ degrees of freedom. Units are expressed in SI; since $1\,\mathrm{mg\,L^{-1}} \equiv 1\,\mathrm{t\,Mm^{-3}}$, the coefficient a_v in mg·L⁻¹ is numerically identical to a per-volume sensitivity in t·Mm⁻³. Residual plots were inspected to check for obvious non-linearity or heteroscedasticity. The calibrated coefficients and their uncertainties are then propagated to per-100 mm sensitivities and site-wide annual increments using scalar error propagation (delta method), i.e. $SE(K_{100}) = V_{100}\, SE_a$ and $CI_{95\%}(K_{100}) = K_{100} \pm t_{0.975,n-2}\, SE(K_{100})$, where V_{100} is the effective infiltration volume associated with +100 mm precipitation. These procedures follow standard treatments of simple linear regression and interval estimation (**Montgomery et. al., 2021**).

Mathematical Model Formulation. Building on column-leaching formulations and hydroclimatic transport-reaction metrics from prior work (**Long et al., 2020; Kumar et al., 2020**), together with similarity π-theorem scaling and leaching time-scale criteria (**Vladyko et al., 2022; Crundwell, 2005**), we formulate a dimensional-analysis framework for cumulative TDS leaching from coal spoil. We first outline the controlling processes and variables retained in the analysis, before assembling them into a compact set of dimensionless groups that couple precipitation forcing and infiltration with pore-scale retention/adsorption and heap geometry, thereby enabling scalable links from column conditions to field-scale predictions (**Long et al., 2020; Kumar et al., 2020; Crundwell, 2005; Vladyko et al., 2022**).

Leaching of SO_4^{2-}, Cl^- and HCO_3^- from coal waste is controlled by meteoric infiltration, mineral structure, and oxidation at the surface. To generalise these effects, we applied dimensional analysis and similarity theory, producing a predictive model of cumulative ion release.

Under the working assumption that the cumulative mass of leached TDS scales with the infiltrated water volume and is modulated by physical characteristics of the spoil heap, we construct a system of dimensionless groups governing the leaching process. These comprise: (i) terms characterising the dependence of TDS mass on precipitation intensity and cumulative volume; (ii) groups combining hydraulic conductivity, leaching duration, porosity, density and water-solid interaction time; and (iii) geometrical and structural descriptors of the spoil that influence transport pathways and retention capacity.

The general non-dimensional form of the model is given by:

$$M_{TDS} = f\left(V_p, V_f, T, S, P_p, m_{ore}, \varepsilon, \rho, k_{ads}\right) \quad (3)$$

Where:

M_{TDS} – total mass of leached TDS over the integration period T within the chosen control volume (column or spoil block) (kg),

V_p – cumulative precipitation volume that falls onto the active infiltration area (S) during (T) (m³),

V_f – effective infiltration volume that actually reaches the reactive pore space (after run-off/evaporation losses) (m³),

T – leaching duration (integration time) (h or d),

S – infiltration area, i.e. the active surface of the spoil (or cross-section in a column set-up) through which water enters the system (m²),

P_p – precipitation intensity, (mm·h⁻¹),

m_{ore} – mass of solid spoil within the control volume that participates in leaching over (T) (kg),

ε – effective (mobile) porosity, the fraction of pore space available to flow, dimensionless (0-1),

ρ – bulk density of the spoil mass, (kg·m⁻³),

k_{ads} – effective adsorption/distribution coefficient (m³·kg⁻¹).

The cumulative precipitation volume is defined as:

$$V_p = S \int_0^T P(t)dt \quad (4)$$

where $P(t)$ is the precipitation intensity (m·h⁻¹), S is the active infiltration area (m²), and T is the integration period (h or d).

For periods with approximately constant mean precipitation intensity P_p, this integral can be approximated as:

$$V_p \approx T \cdot S \cdot P_p \quad (5)$$

The effective infiltration volume is then defined as $V_f = \eta \cdot V_p$, where $0 \le \eta \le 1$ is the infiltration coefficient accounting for runoff and evaporation losses:

$$V_f = \eta \cdot V_p \quad (6)$$

Assuming separable contributions from water flux and solid-phase reactivity, the normalised expression is:

$$\frac{M_{TDS}}{m_{ore}} = f\left(\frac{T \cdot S \cdot P_p \cdot m_{ore}}{V_p \cdot V_f \cdot \rho \cdot \varepsilon}\right) + \varphi\left(\frac{T \cdot S \cdot P_p \cdot m_f}{V_p \cdot V_f \cdot \rho \cdot \varepsilon}\right) \quad (7)$$

Where:

m_f – mass of the sorbing (fine) fraction (kg).

The non-linear function $\varphi(\cdot)$, associated with sorption and secondary mechanisms, can be expanded as:

$$\varphi(\cdot) = c \cdot \frac{T \cdot S \cdot P_p \cdot m_f \cdot k_{ads}}{V_p \cdot V_f \cdot \rho \cdot \varepsilon} + d \cdot \frac{T \cdot S \cdot P_p}{V_p \cdot V_f} + e \cdot k_{ads} \quad (8)$$

Under the assumption that $f\left(\frac{T \cdot S \cdot P_p \cdot m_{ore}}{V_p \cdot V_f \cdot \rho \cdot \varepsilon}\right)$ is *approximately* linear in its argument, the linear component of the model (the first term of **Equation 6**) is:

$$a \cdot \frac{T \cdot S \cdot P_p \cdot m_{ore}}{V_p \cdot V_f \cdot \rho \cdot \varepsilon} \quad (9)$$

where *a, b, c, d*, e are empirical coefficients obtained from laboratory column leaching experiments.

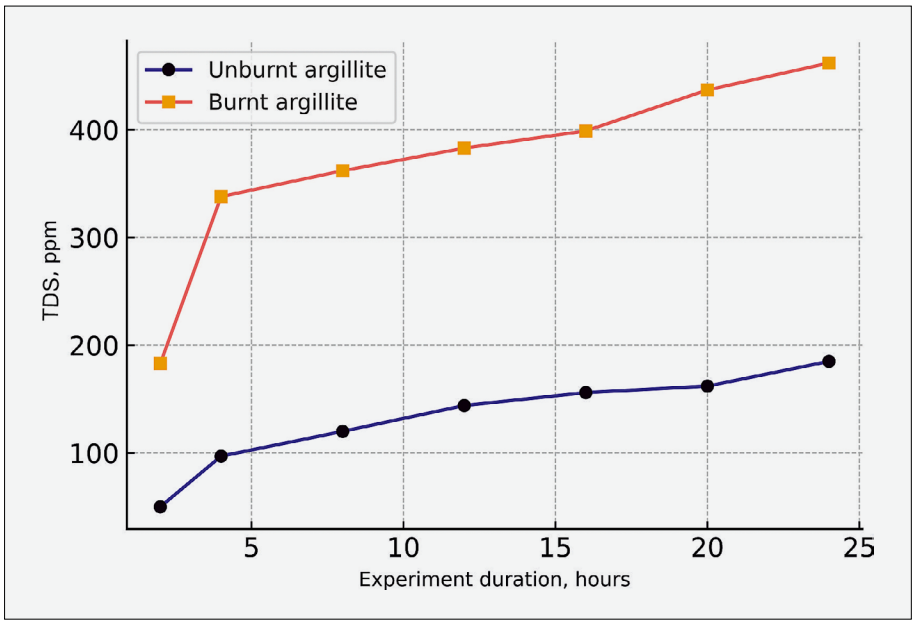

Figure 3. Temporal leaching behaviour of TDS from argillite in a laboratory column test.

The function $\varphi(\cdot)$ is infinitesimal compared with the function f and may therefore be neglected. Therefore, the model can be simplified to the linear approximation:

$$\frac{M_{TDS}}{m_{ore}} \approx a \cdot \frac{T \cdot S \cdot P_p \cdot m_{ore}}{V_p \cdot V_f \cdot \rho \cdot \varepsilon} + b \qquad (10)$$

Whereas this formulation was validated primarily for TDS *in our column experiments*, the same framework is directly transferable to other major ions, provided their leaching behaviour is similarly governed by water input and physical retention. The resulting model enables estimation of contaminant fluxes (expressed, for instance, in kg·Mm^{-3}, equivalent to 10^{-9} kg·m^{-3}) based on precipitation regime, heap structure, and material characteristics, supporting applications in mine site risk assessment and remediation planning. These column-scale metrics provide the empirical basis for the precipitation-based scaling $M_{TDS} = k \cdot P$, which is calibrated and applied to site-wide predictions.

3. Results

3.1. General Leaching Patterns of Major Ions

This section reports laboratory outcomes and translates them into precipitation-scaled predictions for site-wide loads. A comparison of the concentrations of dissolved solids in the leachates from thermally altered (burnt) and unaltered samples shows a much higher concentration of TDS in the burnt material: after 24 h of leaching (8.5 L of deionised water), the TDS content reached 462 mg·L^{-1} in the burnt sample, compared to 185 mg·L^{-1} in the unburnt one (see **Figure 3**). In both materials, a pronounced early-time spike in TDS is observed at ~2 h, after which concentrations decline towards quasi-steady values over the remainder of the 24 h run.

This corresponds to more than double the cumulative mass of dissolved salts - approximately 3.93 g versus 1.57 g. These masses follow directly from the closed recirculating setup: $M=\sum C_j \Delta V_j$ over the 24-h run (see **Equation 1**), which is numerically identical to $C_{final}\times 8.5$ L because the entire dissolved load resides in the tank at the end; equivalently, $M=(M/V)_{avg}\times 432$ L (see **Table 1**).

Differences in leaching behaviour are evident even at the early stages of the experiment. For instance, after only 2 h (≈0.7 L of water), the TDS in the burnt sample reached 183 mg·L^{-1}, which is 3.7 times higher than in the unburnt counterpart (50 mg·L^{-1}).

Analysis of individual ions in the final filtrates confirms this trend (see **Figure 4**). Sulphate (SO_4^{2-}) concentrations in the burnt sample reached 318 mg·L^{-1}, more than double the value observed in the unburnt sample (141.5 mg·L^{-1}). Similar increases were observed for bicarbonates, Ca^{2+}, Mg^{2+}, K^+, and Cl^-.

Conventions. Sulphate (SO_4^{2-}) concentrations are shown **rescaled by ×0.1** to maintain all ions on a common y-axis scale. This rescaling was applied solely for graphical clarity and does not affect the relative trends or ratios among ions.

3.2. Experimental Leaching as a Basis for Model Calibration

The laboratory column leaching test provided the empirical foundation for calibrating the mathematical model that describes TDS release from coal spoil material under rainfall conditions. Specifically, the experimental setup enabled computation of the average leaching of salt ions concentration per unit water volume (M/V, mg·L^{-1}) for unburnt and burnt argillite, as well as the cumulative leached mass. During the 24-hour experiment, 8.5 L of deionised water was passed through each

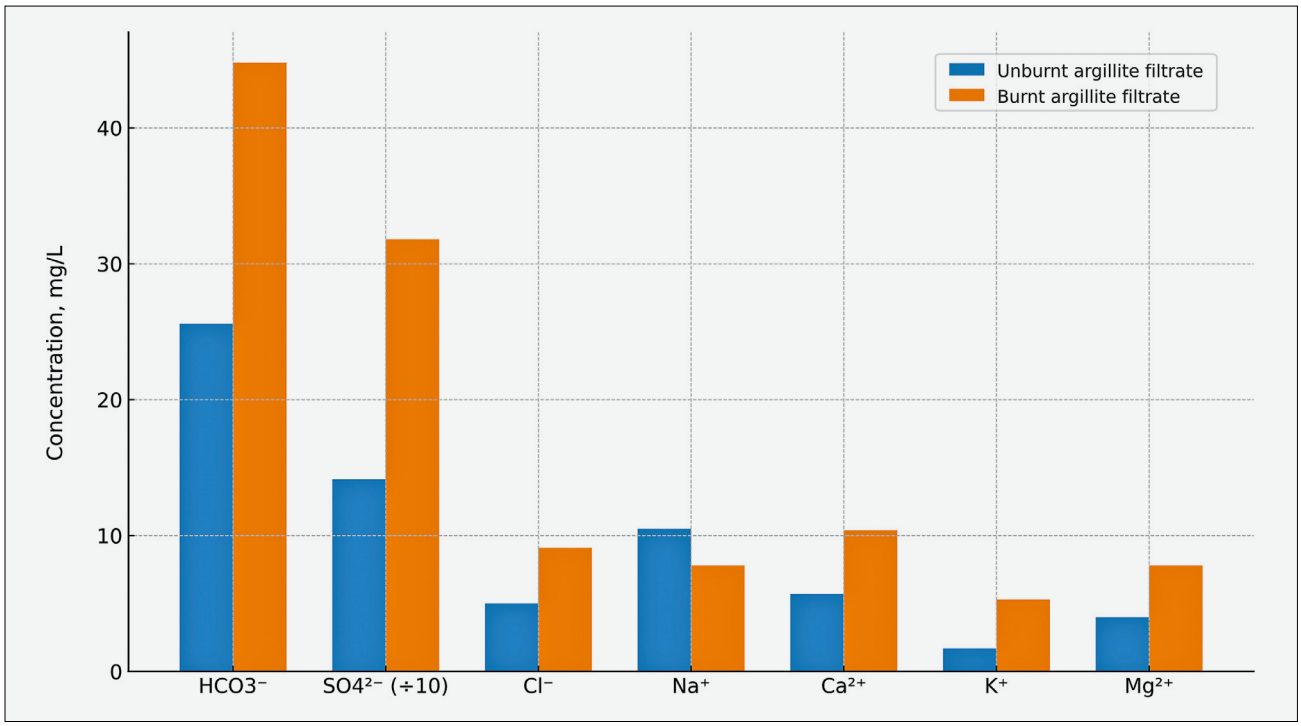

Figure 4. Distribution of water-soluble ions in filtrates of thermally altered and unaltered argillite samples (sulphate bars scaled by ×0.1).

100 g sample under a controlled flow rate of 300 mL·min⁻¹. At the end of the flushing cycle, the cumulative TDS concentration in the filtrate reached 185 mg·L⁻¹ for the unburnt sample and 462 mg·L⁻¹ for the thermally altered (burnt) one. These values correspond to cumulative leached masses of approximately 1.57 g and 3.93 g per sample, respectively.

Table 1. Column leaching results for unburnt and burnt argillite samples (24 h circulation; 8.5 L deionised water; 100 g material).

Parameter	Unburnt Argillite	Burnt Argillite
Mass of sample (g)	100	100
Volume of leachant (L)	8.5	8.5
Total filtrate passed (L)	432	432
Total TDS leached (mg)	1572.5	3927.0
Average *M/V* over total passed volume, (mg·L⁻¹)	3.64	9.09
Final TDS in filtrate (mg·L⁻¹)	185	462

Conventions. Average *M/V* is computed as total leached mass divided by the total passed volume (V_{total} = 432 L). Final TDS in filtrate refers to the concentration measured in the last collected solution portion.

Assuming a linear relationship between water volume and salt release over the tested range, the average TDS per unit water volume was computed as *M/V* (units: mg·L⁻¹); detailed values are reported in **Table 1**. Given the geometric characteristics of the test columns (cross-sectional area ≈ 0.001 m²), the corresponding **column-scale areal fluxes** were approximately J_{24h}≈1570 g m⁻² day⁻¹ (unburnt) and J_{24h}≈3930 g m⁻² day⁻¹ (burnt), computed as J_{24h}=*M*/(*A*·24 h) using the column cross-section.

These experimentally derived column metrics (*M, V,* and *M/V*) informed the calibration of the precipitation-based model, which was then used to simulate TDS leaching as a function of annual precipitation. **Table 1** summarises the primary data and calculations used for model calibration. This ensured consistency between laboratory observations and the field-scale predictive framework.

Table 2. Linear regression diagnostics for *M–V* calibration (column experiments)

Treatment	a_v (slope, mg·L⁻¹ = t·Mm⁻³)	SE_a (mg·L⁻¹)	95% CI for a_v (mg·L⁻¹)	b_v (intercept, mg)	SE_b (mg)	R^2
Unburn	190.94	9.81	[165.70, 216.18]	−156.38	50.26	0.987
Burnt	474.40	18.79	[426.07, 522.73]	−274.74	96.30	0.992

Conventions. (i) Units: a_v in mg·L⁻¹ are numerically equivalent to t·Mm⁻³ (since 1 mg L⁻¹ = 1 t Mm⁻³). (ii) 95% CI computed as $a_v \pm t_{0.975,n-2}\, SE_a$ (here $t_{0.975,5} = 2.571$). (iii) Intercepts reflect linear extrapolation towards $V \to 0$ and are not used for site-scale projections.

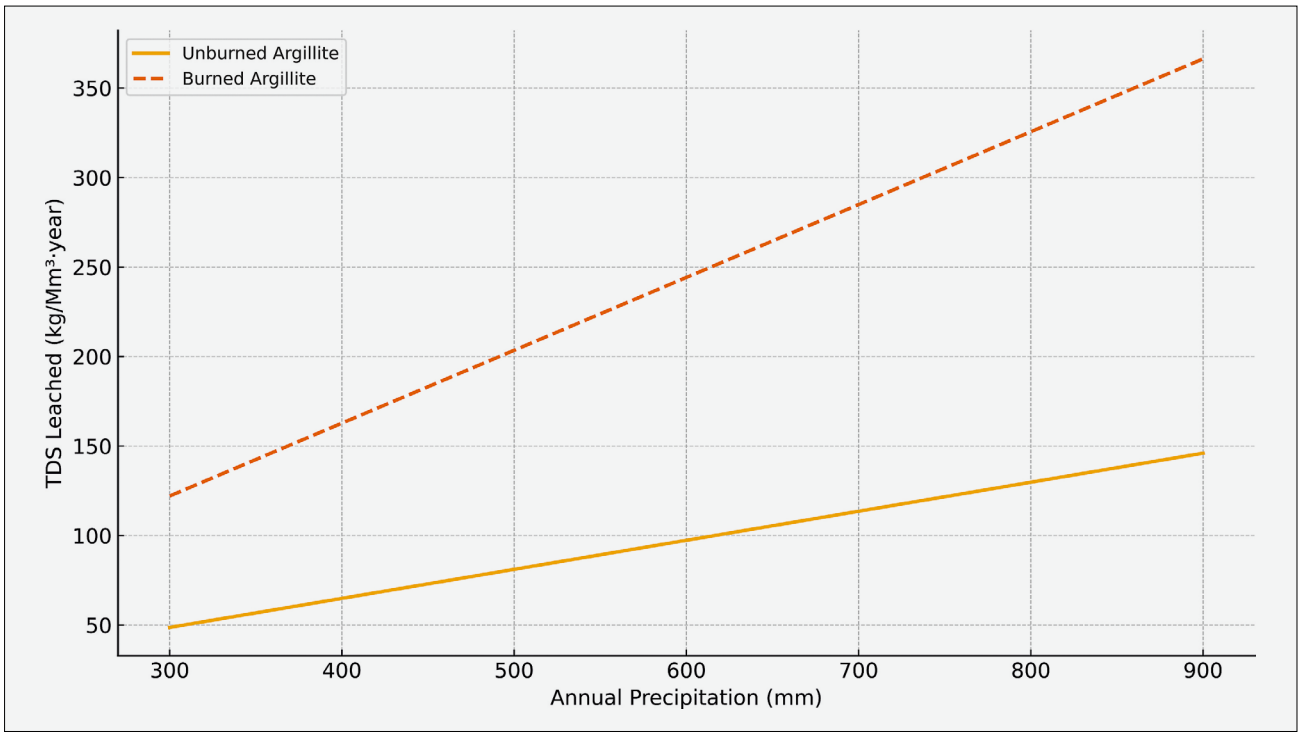

Figure 5. Sensitivity of per-volume TDS release to precipitation: comparison of unburnt vs. burnt argillite.

To quantify linearity and propagate uncertainty into the site-scale model, the cumulative mass-volume relation was fitted as $M = a_v V + b_v$ for each treatment. The regression diagnostics-slope (a_v), standard error of the slope (SE_a), 95% confidence interval, intercept (b_v), its standard error, the coefficient of determination (R^2) and sample size (n) – are compiled in **Table 2**.

3.3. *Precipitation-TDS response and sensitivity (per-volume and site-scale)*

As a result of the mathematical modelling, we quantified the relationship between annual precipitation P (mm·yr^{-1}) and the annual TDS release per unit spoil volume M_{TDS} (t·Mm^{-3}·yr^{-1}) for unburnt and burnt argillite (see **Figure 5**).

For clarity, the relations used in **Figure 5** are written explicitly as:

$$M_{TDS\ unburnt} = 3.31 \times 10^{-3} \cdot P \quad (11)$$

$$M_{TDS\ burnt} = 8.78 \times 10^{-3} \cdot P \quad (12)$$

with slope parameters $k_{unburnt}$=3.31×10^{-3} and k_{burnt}= 8.78×10^{-3}. Across the tested precipitation range, the model yielded approximately 1.0-3.0 t·Mm^{-3}·yr^{-1} for unburnt and approximately 2.6-7.9 t·Mm^{-3}·yr^{-1} for burnt argillite, confirming a monotonic response and consistently higher release for thermally altered material.

In this precipitation-based representation (per-volume release vs. annual P), the burnt/unburnt slope ratio equals $k_{burnt}/k_{unburnt}$=2.653. At the column scale, however, the corresponding ratios obtained from independent metrics are close to ≈2.50: final filtrate concentrations were 462 vs. 185 mg·L^{-1} (ratio 2.497), and cumulative leached masses were 3.93 vs. 1.57 g (ratio 2.503). Using a constant column cross-section of 0.001018 m², these masses imply areal fluxes of ≈ 3930 vs. ≈ 1570 g·m^{-2} per 24 h (ratio 2.497). Taken together, the burnt/unburnt ratio is **metric-dependent** (concentration, mass, areal flux, or precipitation-based per-volume release) and should therefore be interpreted strictly within the normalisation used in each plot.

Model-based scaling using calibrated coefficients; areal annual fluxes Jyear are reported in the text for each scenario.

Site-wide scaling. Using the column-calibrated coefficients *a, b* and the site parameters (S_{site}, $m_{ore,site}$,, ρ, ε), the annual mass export of dissolved solids is estimated from precipitation as:

$$V_{p,site} = S_{site} P_{tot} \quad (13)$$

$$V_{f,site} = \eta V_{p,site} \quad (14)$$

where P_{tot} is the annual precipitation depth (m·yr^{-1}) and $0 < \eta < 1$ is the effective infiltration coefficient.

Results are expressed as mass load per year (e.g., t·yr^{-1}) and, where required, as areal annual flux:

$$J_{year} = \frac{M_{\mathrm{TDS},site}}{S_{site}\, T} \quad (15)$$

(e.g. kg·m^{-2}·yr^{-1}), enabling comparison across spoil heaps of different size and morphology. Formally, the **areal annual flux** is:

Table 3. Scenario TDS loads vs. annual precipitation (CCCP heap)

Scenario	P (mm·yr⁻¹)	Unburnt M_{TDS} (t·Mm⁻³·yr⁻¹)	Burnt M_{TDS} (t·Mm⁻³·yr⁻¹)	Unburnt site-wide (t·yr⁻¹)	Burnt site-wide (t·yr⁻¹)	Δ vs. 670 mm (Unburnt, t·yr⁻¹)	Δ vs. 670 mm (Burnt, t·yr⁻¹)
Dry	511	1.69	4.49	82.69	219.35	-25.73	-68.25
Average	670	2.22	5.88	108.42	287.60	+0.00	+0.00
Wet	829	2.74	7.28	134.15	355.85	+25.73	+68.25

Conventions. (i) Units: per-volume values in t·Mm⁻³·yr⁻¹; site-wide totals assume V = 48.89 Mm³. (ii) Relations: M_{TDS}, unburnt = 3.31×10⁻³·P, M_{TDS}, burnt = 8.78×10⁻³·P; P in mm·yr⁻¹.

Table 4. Fixed marginal sensitivity (linear model)

Metric	Unburnt	Burnt
Per-volume increment per +100 mm (t·Mm⁻³·yr⁻¹)	0.33	0.88
Site-wide increment per +100 mm (t·yr⁻¹)	16.18	42.93

$$J_{year} = \frac{M_{TDS,site}}{S_{site} \cdot 1_{yr}} \quad (\mathrm{kg \cdot m^{-2} yr^{-1}}) \qquad (16)$$

For S_{site} = 0.8638 km², the scenario values are: **Dry (511 mm)** – J_{year} ≈ 0.096 (unburnt) and 0.254 (burnt); **Average (670 mm)** – 0.1260 (unburnt) and 0.333 (burnt); **Wet (829 mm)** – 0.155 (unburnt) and 0.412 (burnt) kg·m⁻²·yr⁻¹.

For each additional 100 mm of annual precipitation, the predicted release increases by 0.331 t·Mm⁻³·yr⁻¹ for unburnt and 0.878 t·Mm⁻³·yr⁻¹ for burnt argillite. When scaled by the CCCP spoil volume V=48.89 Mm³, these per-100 mm sensitivities correspond to **+16.18 t·yr⁻¹** (unburnt) and **+42.93 t·yr⁻¹** (burnt) in site-wide annual loads. These sensitivities are constant within the applicability domain of the adopted linear approximation; slope values and their ratio will differ if a different metric or normalisation is used, which is why the specific definition is provided alongside each figure.

To operationalise the linear precipitation – TDS relations reported above, **Table 3** summarises per-volume responses and the corresponding site-wide annual loads for three precipitation scenarios spanning the CCCP site range, while **Table 4** lists the fixed marginal sensitivities per +100 mm of precipitation.

Table 3 summarises the per-volume model M_{TDS} = k·P and the corresponding site-wide annual loads for three representative precipitation scenarios – Dry (511 mm), Average (670 mm) and Wet (829 mm). These values confirm a monotonic increase with P and consistently higher magnitudes for burnt argillite. Relative to the Average scenario (670 mm), the Dry scenario reduces the site-wide load by − 25.73 t·yr⁻¹ (unburnt) and – 68.25 t·yr⁻¹ (burnt), whereas the Wet scenario increases it by +25.73 t·yr⁻¹ and +68.25 t·yr⁻¹, respectively. Across the full span from 511 to 829 mm, the site-wide TDS load rises by 51.46 t·yr⁻¹ (unburnt) and 136.50 t·yr⁻¹ (burnt).

*According to **Table 4**, the constant increments implied by the linear model per +100 mm of annual precipitation are summarised.* This tabular presentation facilitates straightforward application of the model to varying climatic scenarios without the need for recalculation. These increments are invariant within the calibration domain and can be used to interpolate between scenarios or to adjust loads for intermediate P. They also facilitate quick updates using observed or forecast precipitation without re-fitting the model. For instance, +200-300 mm above mean annual precipitation would increase site-wide TDS export by ≈32-64 t·yr⁻¹ for unburnt-dominant scenarios and ≈ 86-129 t·yr⁻¹ where burnt materials prevail.

Building directly on the per-volume precipitation - TDS relations (**Equations 11-12; Figure 5**), our results show a robust, approximately linear increase of annual salt release with increasing annual precipitation for both lithological states of argillite, with consistently higher magnitudes for thermally altered (burnt) material. The slope parameters $k_{unburnt}$ = 3.31×10⁻³ and k_{burnt} = 8.78×10⁻³ (t·Mm⁻³·mm⁻¹) quantify this contrast and, together with the site-scale volume of the CCCP spoil heap, allow direct translation from climatic variability to annual salt loads. This contrast between burnt and unburnt rock is consistent with the results of our earlier studies (**Kochmar and Karabyn, 2023**).

3.4. Ion-specific response of leaching to precipitation

Building on the linear precipitation-TDS relations described in Section 3.3, we apportioned the precipitation-driven release to individual dissolved species using the final filtrate composition from the column experiments (see **Table 5**). **For each material regime** m **(unburnt or burnt), we treat the leachate composition as quasi-stationary, i.e.** $c_i(t) \approx \alpha_{i,m}\, c_{TDS}(t)$. **We compute** $\alpha_{i,m}$ **from the final tank composition as** $\alpha_{i,m} = C_{i,final} / \sum_{j \in J} C_{j,final}$ **over the major ions listed in Table 5, so that** $\sum_i \alpha_{i,m} = 1$. **Integrating the mass balance** $M_i = \int c_i\, dV$ **gives** $M_i = \alpha_{i,m} M_{TDS}$**; together with** $M_{TDS} = k_{TDS,m} P$ **and** $M_i = k_{i,m} P$**, this yields** $k_{i,m} = \alpha_{i,m} k_{TDS,m}$**. For transparency, we also report** $\sum_i \alpha_{i,m}$ **and the variability of** C_i/C_{TDS} **across samples (median and coefficient of variation) to document the quasi-stationarity assumption.** Here, $\alpha_{i,m}$

denotes the mass fraction of ion i among the major ions in the filtrate of material m (HCO_3^-, SO_4^{2-}, Cl^-, Na^+, K^+, Mg^{2+}, Ca^{2+}), and $k_{TDS,m}$ is the precipitation-based slope ($k_{unburnt} = 3.31 \times 10^{-3}$; $k_{burnt} = 8.78 \times 10^{-3}$ t·Mm^{-3}·mm^{-1}). The fractions are normalised to sum to unity, ensuring that $\Sigma_i k_{i,m} = k_{TDS,m}$. The resulting composition weights are: burnt argillite dominated by sulphate (≈79%) with bicarbonate ≈11%; unburnt argillite ≈72% sulphate and ≈13% bicarbonate; alkali and alkaline-earth cations (Na^+, K^+, Mg^{2+}, Ca^{2+}) contribute only a few per cent each.

Table 5. Major-ion shares in the filtrate, used for partitioning the TDS slope

Ion	Unburnt (%)	Burnt (%)
HCO_3^-	13.0	11.1
SO_4^{2-}	71.7	78.6
Cl^-	2.5	2.2
Na^+	5.3	1.9
K^+	0.9	1.3
Mg^{2+}	2.0	1.9
Ca^{2+}	2.9	2.6

Conventions. (i) Fractions ($\alpha_{i,m}$, %) are calculated from the major-ion concentrations and normalised within the major-ion set. (ii) For unburnt material, Cl^- is treated as 5.0 mg·L^{-1} (upper bound).

To complement the composition weights in **Table 5**, **Table 6** presents the marginal sensitivities per +100 mm of precipitation for individual ions, reported both as per-volume and site-wide values.

Building on these marginal sensitivities, **Table 7** presents the predicted annual releases of major ions at a representative precipitation level of 670 mm·yr^{-1}, expressed both per-volume and as site-wide loads.

Sulphate dominates the precipitation-driven response in both materials, contributing ≈72% (unburnt) and ≈79% (burnt) of the bulk TDS slope. The bicarbonate fraction is 11-13%, consistent with carbonate buffering and dissolution. Among cations, Ca^{2+} and Mg^{2+} increments are modest but non-negligible. Since the model is linear, the difference in ion release between dry years (511 mm) and wet years (829 mm) can be obtained directly by multiplying the +100 mm sensitivities from **Table 6** by the corresponding precipitation difference. As a reference point, **Table 7** summarises the predicted annual releases of major ions at 670 mm·yr^{-1} (the average precipitation scenario), showing that sulphate overwhelmingly dominates the total loads, followed by bicarbonate, with other cations contributing only marginally. This linearity assumption simplifies projections but may under-represent potential nonlinear responses during extreme hydrological events.

Table 6. Marginal increase in annual load per +100 mm of precipitation (ΔP = 100 mm).

Ion	Unburnt (per-volume, t·Mm^{-3}·yr^{-1} per +100 mm)	Burnt (per-volume, t·Mm^{-3}·yr^{-1} per +100 mm)	Unburnt (site-wide, t·yr^{-1} per +100 mm)	Burnt (site-wide, t·yr^{-1} per +100 mm)
HCO_3^-	0.043	0.097	2.10	4.75
SO_4^{2-}	0.237	0.690	11.61	33.74
Cl^-	0.008	0.020	0.41	0.97
Na^+	0.018	0.017	0.86	0.83
K^+	0.003	0.012	0.14	0.56
Mg^{2+}	0.007	0.017	0.33	0.83
Ca^{2+}	0.010	0.023	0.47	1.10

Conventions.Values are reported both as per-volume (t·Mm^{-3}·yr^{-1} per +100 mm) and as site-wide increments (t·yr^{-1} per +100 mm), assuming a spoil volume of V = 48.89 Mm³.

Table 7. Predicted major-ion releases at P = 670 mm·yr^{-1}

Ion	Unburnt (t·Mm^{-3}·yr^{-1}; t·yr^{-1})	Burnt (t·Mm^{-3}·yr^{-1}; t·yr^{-1})
HCO_3^-	0.288 (14.07)	0.651 (31.84)
SO_4^{2-}	1.590 (77.76)	4.623 (226.04)
Cl^-	0.056 (2.75)	0.132 (6.45)
Na^+	0.118 (5.77)	0.113 (5.54)
K^+	0.019 (0.94)	0.077 (3.76)
Mg^{2+}	0.045 (2.19)	0.113 (5.53)
Ca^{2+}	0.064 (3.13)	0.151 (7.39)

Conventions. Values are reported as per-volume rates $\Delta M_i/V$ (t·Mm^{-3}·yr^{-1}) and as site-wide loads ΔM_i (t·yr^{-1}, in parentheses), computed for a spoil volume of V = 48.89 Mm³.

This equal-rate assumption follows the linear relationship $M_{TDS} = kTDS, m{\cdot}P$. These methodological choices do not affect additivity or the dominant sulphate signal, but they should be reconsidered if time-resolved compositions become available. The results have direct implications for anticipating water-quality impacts under extreme precipitation scenarios, which may escalate into local emergency situations requiring civil protection measures. Furthermore, the ion-resolved relationships established here underpin the scenario analysis linking climatic variability to composition-specific load changes. These quantified responses and sensitivities are inter-

preted in the context of mechanisms, published ranges, and implications for civil protection. These quantified responses and sensitivities are interpreted below in the context of mechanisms, published ranges, and implications for civil protection.

4. Discussion

4.1.-Leaching mechanisms

The approximately linear precipitation-TDS relation indicates that annual salt export is primarily water-flux-limited, whereas thermally altered argillite exhibits higher reactivity across scales. Two features are salient: (i) fixed marginal sensitivities enable scenario-based extrapolation across climatic regimes; and (ii) the magnitude of the burnt-unburnt contrast is contingent on the normalisation of the response metric (per spoil volume, per water volume, or per exposed area).

Thermal alteration augments salt release by breaking mineral lattices and exposing fresh reactive surfaces, by oxidising sulphides (e.g. pyrite) and promoting formation of readily soluble sulphate-bearing secondary phases (e.g. gypsum, anhydrite), and by altering pore architecture toward higher connectivity for percolating water (**Castillo-Meza et al., 2020; Gao et al., 2025**). Coal-spoil studies show higher SC/TDS ratios and sulphate-chloride fluxes from thermally altered (self-heated) materials in both column and field settings (**Daniels et al., 2016b; Orndorff et al., 2015; Clark et al., 2017**).

These pathways are consistent with the elevated sulphate and chloride measured in burnt filtrates and with widely observed increases in ionic strength from thermally affected mine wastes (**Daniels et al., 2016a; Clark et al., 2017; Welch et al., 2021**). In our columns, burnt material exhibits larger initial concentrations and cumulative masses than unburnt material under the same water input, supporting the interpretation that a thermally produced pool of labile salts is efficiently mobilised during wetting cycles. The persistence of a steeper precipitation-response slope in the annual model suggests that, beyond this transient pool, thermally altered rock maintains higher long-term reactivity. At other regional landfills, such as the Nadiya mine spoil tip, concentrations of major ions are also elevated, indicating that coal industry waste is a regional source of pollution throughout the Lviv-Volyn coal basin (**Skrobala et al., 2022**).

A sharp TDS peak around 2 hours (see **Figure 3**) reflects the rapid dissolution and wash-off of soluble secondary salts accumulated on reactive near-surface materials. The concentration then reduces as these salts are depleted and flow stabilises. Field and analogue studies of mine pools associate this 'first flush' to dissolution of efflorescent sulphate salts formed during oxidation. These salts produce highly mineralised waters at the onset of flushing, followed by a gradual reduction in concentrations (**Mugova et al., 2024**). Column tests on empty rock also show an 'early weathering' stage, characterised by high specific conductivity and peak ion concentrations, indicating rapid mobilisation of soluble salts prior to slower, reaction-limited release from less reactive phases (**Martin & Langman, 2024**). This interpretation aligns with the observed post-peak decline in our columns and supports treating early-time pulses as transient contributions superimposed on the longer-term, precipitation-modulated leaching captured by the linear model (**Merritt & Power, 2022**).

These findings align with laboratory and field evidence from other coal basins. Column studies on Appalachian spoils show high early-time TDS and specific conductance that decline toward quasi-steady levels after multiple pore-volume flushes, with higher values for unweathered, sulphide-rich mudstones and black shales (**Orndorff et al., 2015; Daniels et al., 2016b**). Work on closure salinity risk likewise documents rapid declines in Na-Cl where halite is initially present, followed by longer-term sulphate-dominated leaching (**Park et al., 2013**). Weathering-cycle simulations demonstrate that fine-grained fractions can produce extremely high initial TDS pulses that collapse after repeated wetting-drying cycles (**Dang et al., 2019**). At field scale, lysimeter and catchment monitoring confirm the same direction of change but over years to decades, with typical SC declining from >1000 - 3000 $\mu S \cdot cm^{-1}$ to 300 - 700 $\mu S \cdot cm^{-1}$, depending on lithology and management (**EPA, 2011; Daniels et al., 2016a; Welch et al., 2021**). Against this backdrop, our burnt/unburnt contrasts (≈2.5 at column scale; 2.653 at precipitation-based per-volume scale) fall within reported ranges.

4.2. Model adequacy and emergency risks

The linear precipitation-response model adopted in Section 3.3 aligns with established hydrological theory. In chemostatic catchments, solute concentrations vary only weakly with discharge, so annual loads scale approximately linearly with water flux; this behaviour is well documented and has been reaffirmed in recent reassessments (**Godsey et al., 2009**). At broader hydroclimatic scales, export vulnerability is governed by transport-reaction time-scale ratios (a Damköhler-type control), which implies stronger mass mobilisation with greater water inputs across realistic precipitation ranges (**Kumar et al., 2020**). These lines of evidence provide a physically consistent basis for a linear precipitation-mass relation and justify its application to the tested materials and site-relevant precipitation regime (**Godsey et al., 2009, Knapp et al., 2024; Kumar et al., 2020**).

From a civil protection perspective, the constant marginal sensitivities imply that wet-year anomalies translate linearly into elevated TDS loads, with a stronger effect for burnt zones. Wet-year anomalies will proportionally increase site-wide loads, with stronger effects where burnt materials prevail. For instance, +200-300 mm above mean annual precipitation would increase

site-wide TDS export by ≈32-64 t·yr^{-1} for unburnt-dominant scenarios and ≈ 86-129 t·yr^{-1} where burnt materials prevail. Since sulphate and chloride remain mobile under neutral to mildly alkaline conditions, such increases can influence ionic strength, cation exchange, metal speciation, and downstream aquatic ecology (**Daniels et al., 2016a; EPA, 2011; Welch et al., 2021**). These risks may escalate into local environmental emergencies, underscoring the need for preventive measures such as stabilisation of burnt sectors, interception of first-flush leachates, selective covers where f_b is high, and monitoring of SC and sulphate with thresholds informed by per-100 mm sensitivities.

4.3. Model limitations and future directions

The discussion reconciles column-scale evidence and a parsimonious precipitation-response model into a coherent picture of salt leaching from coal-derived argillites. Thermal alteration emerges as the principal intensifier, with effects that are visible across metrics and preserved after scale-up to annual, per-volume predictions. The linear form captures first-order climatic control while remaining transparent enough to support decision-making: every +100 mm of precipitation implies a fixed, material-specific increase in annual TDS export per-volume of spoil and, by extension, a predictable increment in site-wide load at the heap scale.

Methodologically, the approach integrates controlled column leaching (100 g samples, 24 h, 300 mL·min^{-1} flow rate, ≈ 432 L cumulative throughput) with dimensional analysis and simple scaling to the spoil-heap volume (48.89 Mm³). The model thus links micro-scale leaching processes with meso- and macroscale hydrological forcing, allowing the evaluation of salinity export in a form directly applicable to early-warning and planning frameworks of civil protection.

The framework developed here is not limited to the Chervonohrad district. Its formulation is transferable to other spoil piles and mining waste facilities across Ukraine, particularly in eastern regions where spontaneous combustion, shelling, and extreme precipitation combine to create conditions of heightened risk. In such settings, thermal alteration and hydrologic forcing interact to intensify contaminant release, underscoring the importance of a predictive tool that can quantify expected load increments under different climatic scenarios. Extending application to eastern Ukraine provides an opportunity to support civil protection planning under conditions of ongoing military threat. The ability to forecast ion-specific releases strengthens preparedness for potential emergency situations, where contaminated runoff or groundwater could directly impact local communities and ecosystems.

Several limitations should be noted. First, depth coverage was restricted to **0.2 - 0.3 m,** which targets the **near-surface leaching** zone rather than the full vertical variability of **element mobility** within the heap. This upper horizon is hydrologically responsive and biologically active - where infiltration, oxygen exchange and temperature fluctuations enhance sulphide oxidation, dissolution of readily soluble salts, and mobilisation of major ions (notably SO_4^{2-}, Cl^-, HCO_3^-) into percolating waters - yet it does not resolve potential deeper pathways of mobilisation governed by compaction, moisture storage and redox stratification. Accordingly, the reported leachate chemistry should be interpreted as **characteristic of the active near-surface source zone** for first-flush export, with recognition that metre-scale subsurface processes - including low-temperature oxidation and self-heating fronts - may develop below the surface and alter migration pathways and fluxes at depth (**Espinha Marques et al., 2024; Anghelescu & Diaconu, 2024**).

The relationship between the sediment and the mass applied in this study represents a linear approximation of a more general model, in which non-linear sorption and secondary processes are grouped into a term $\varphi(\cdot)$. In this analysis $\varphi(\cdot)$ is set to zero, giving the simplified form used in further modelling. The approach was validated mainly for total dissolved solids using recirculating column experiments, and ion-specific loads were estimated by applying quasi-stationary composition weights. Additional uncertainty arises at field scale from **hydrological** representation and scale transition: runoff generation, preferential flow and seasonal storage can decouple precipitation from effective infiltration; stratification and patchiness within spoil heaps may bias scaling; and column geometries differ from field conditions. Accordingly, confidence intervals should be propagated when translating **per-volume** sensitivities into **site-wide** annual loads for risk management. Finally, the fixed **per-100 mm** sensitivities should be applied as constants only within the stated applicability and calibration domain of the linear model.

In summary, the synthesis highlights both the mechanistic insight and the applied relevance of the model. It provides a robust, adaptable framework for environmental management in mining regions and a practical foundation for integrated civil protection strategies across Ukraine and beyond.

Future work should aim to extend the modelling framework beyond the CCCP heap, applying it to other spoil piles and concentration plant dumps across Ukraine, particularly in the eastern regions that are subject to shelling and therefore present higher risks than the Chervonohrad district. Further developments should also integrate a dynamic water balance module that translates precipitation into effective infiltration as a function of cover, slope, and season. In order to implement such approaches under real constraints, optimisation based on dynamic programming is an effective method for selecting and sequencing technological actions (**Lousada et al., 2024**). In addition, model calibration should be extended not only to total TDS, but also separately to sulphates, bicarbonates and chlorides. Such

improvements will enhance the accuracy and reliability of the model and will be useful in planning civil protection measures for mining regions.

4.4.-Recommendations

Given the calibrated linear precipitation–TDS response ($k_{unburnt}$ = 3.31 × 10^{-3} and k_{burnt} = 8.78 × 10^{-3} t·Mm^{-3}·mm^{-1}) and the fixed marginal sensitivities per +100 mm of annual precipitation (+0.331 and +0.878 t·Mm^{-3}·yr^{-1}; site-wide +16.18 and +42.93 t·yr^{-1} for unburnt and burnt material, respectively), management should prioritise (i) stabilisation and hydrologic control of thermally altered (burnt) sectors, where per-volume slopes and loads are consistently higher; (ii) interception of first-flush leachates during heavy rainfall and snowmelt, as early-time pulses dominate short-term export; (iii) routine monitoring of specific conductance and sulphate as pragmatic early-warning indicators, with action thresholds derived directly from the +100 mm sensitivities in **Table 4** and the precipitation scenarios in **Table 3**; (iv) selective covers and drainage measures in areas with high effective infiltration (η), to reduce *Vf* and thus annual loads; and (v) contingency planning for wet-year anomalies (+200 – 300 mm), which, under linear scaling, translate into predictable tens-of-tonnes increases in site-wide TDS export. These measures follow directly from the observed burnt/unburnt contrasts, the linear precipitation dependence over the site-relevant range, and the ion partitioning that highlights sulphate as the dominant contributor to annual loads.

5. Conclusions

This study developed and applied an integrated mathematical and physical modelling framework to quantify the leaching dynamics of salt ions from coal-mining waste, with particular emphasis on the contrasting behaviours of thermally altered (burnt) and unaltered (unburnt) argillite. By linking controlled column experiments with a precipitation-response model scaled to the CCCP spoil heap, we demonstrated that annual releases of TDS increase linearly with precipitation input, and that burnt materials consistently exhibit higher fluxes across multiple metrics. This outcome reflects both the mobilisation of labile salts and the sustained reactivity of sulphide-bearing phases subjected to thermal alteration.

The analysis of ion-specific contributions revealed that sulphate overwhelmingly dominates the precipitation-driven signal (≈ 72 - 79%), with bicarbonate providing secondary buffering and other cations contributing marginally. This composition indicates that environmental risks from coal-mining waste leachates are not uniformly distributed among ions but are heavily shaped by sulphate oxidation processes, which directly threaten ecological safety through elevated ionic strength, potential metal mobilisation, and downstream impacts on aquatic systems.

From a methodological standpoint, the use of linear precipitation-response functions provides a parsimonious yet robust predictor of annual TDS loads, facilitating the translation of climatic variability into site-wide estimates of pollutant release. Such predictive capacity is essential for integrating hydrogeochemical insights into risk assessments and early-warning systems for civil protection. Collected sensitivity data (+0.331 and +0.878 t Mm^{-3} yr^{-1} per +100 mm for unburnt and burnt argillite, respectively) provide practical thresholds for scenario planning across dry, average, and wet-year conditions.

Coal-mining waste heaps are not only local sources of salinity but can also trigger environmental emergencies during extreme hydrological events. Linear upscaling indicates that wet-year anomalies (+200–300 mm) may increase site-wide TDS exports by tens of tonnes per year – a load high enough to stress receiving waters. These results suggest that spoil-heap leaching should be included in regional strategies for emergency readiness and civil protection.

For civil protection and ecological safety planning in Ukraine and other coal mining regions, particularly those exposed to armed conflict and the associated risks of spontaneous combustion, the findings underscore several priorities. First, stabilisation and hydrological control of thermally altered sectors are essential to minimise salt ions leaching. Second, interception of first-flush leachates during heavy rainfall and snowmelt can substantially reduce the load of dissolved salts reaching receiving waters. Third, continuous monitoring of sulphate and electrical conductivity should be implemented as early-warning indicators, ensuring timely detection of elevated releases. These measures are critical to reducing vulnerability to environmental emergencies and strengthening adaptive capacity.

Overall, the modelling framework presented here is transferable beyond the Chervonohrad region. It provides a generic yet adaptable tool for anticipating the mobilisation of dissolved loads from coal-derived wastes under variable climatic forcing. The study not only advances hydrogeochemical science but also directly supports the development of integrated environmental-civil protection systems, thereby bridging ecological research with applied disaster risk reduction in mining-affected landscapes.

6. References

Alvarenga, P., Guerreiro, N., Simões, I., Imaginário, M. J. and Palma, P. (2021). Assessment of the environmental impact of acid mine drainage on surface water, stream sediments, and macrophytes using a battery of chemical and ecotoxicological indicators. Water, 13(10), 1436. https://doi.org/10.3390/w13101436

American Public Health Association (APHA), American Water Works Association (AWWA), & Water Environment Federation (WEF). (2017). Standard Methods for the Ex-

amination of Water and Wastewater (23rd ed.). Washington, DC: APHA-AWWA-WEF.

Anghelescu, L., and Diaconu, B. M. (2024). Advances in detection and monitoring of coal spontaneous combustion: Techniques, challenges, and future directions. Fire, *7*(10), 354. https://doi.org/10.3390/fire7100354

Bosak, P., Popovych, V., Stepova, K. and Dudyn, R. (2020). Environmental impact and toxicological properties of mine dumps of the Lviv-Volyn coal basin. News of the National Academy of Sciences of the Republic of Kazakhstan, Series of Geology and Technical Sciences, 2(440), 48-54. https://doi.org/10.32014/2020.2518-170X.30

Castillo-Meza, A.J., Daniels, W.L., Zipper, C.E. and Orndorff, Z.W. (2020). Estimating total dissolved solids release from coal mine spoils using laboratory leaching procedures. International Journal of Coal Geology, 218, 103353. https://doi.org/10.1016/j.coal.2019.103353

Clark, G. M., Daniels, W. L., Orndorff, Z.W. and Zipper, C.E. (2017). Thermal alteration and leaching dynamics in Appalachian coal spoil piles. Applied Geochemistry, 82, 125-138. https://doi.org/10.1016/j.apgeochem.2017.05.012

Cooke, C. A., Emmerton, C. A., Donahue, W. F., & Kerr, J. G. (2025). Downstream water quality impacts persist despite mountaintop coal mine reclamation in the Canadian Rocky Mountains. *Environmental Pollution*, *383*, 126841. https://doi.org/10.1016/j.envpol.2025.126841

Crundwell, F.K. (2005). The leaching number: its definition and use in determining the performance of leaching reactors and autoclaves. Minerals Engineering, 18(13-14), 1315-1324. https://doi.org/10.1016/j.mineng.2005.06.014

Dang, Z., Li, P., Edraki, M. and Huang, L. (2019). The effect of weathering on salt release from coal mine spoils. Minerals, 9(12), 760. https://doi.org/10.3390/min9120760

Daniels, W.L., Orndorff, Z.W., Zipper, C.E. and Beck, M.A. (2016a). Column and field-scale leaching of treated and untreated coal spoils: sulphate mobilisation post-heating. Journal of Environmental Quality, 45(3), 743-753. https://doi.org/10.2134/jeq2015.06.0313

Daniels, W.L., Zipper, C.E., Orndorff, Z.W., Skousen, J., Barton, C.D., McDonald, L.M. and Beck, M.A. (2016b). Predicting total dissolved solids release from central Appalachian coal mine spoils. Environmental Pollution, 216, 371-379. https://doi.org/10.1016/j.envpol.2016.05.044

EPA. (2011). A field-based study of TDS impacts on benthic macroinvertebrate communities in central Appalachian streams. EPA/600/R-09/138F. https://www.epa.gov/sites/default/files/2015-03/documents/final_tds_report_1333.pdf

Espinha Marques, J., Narayan, A., Santos, P., Ribeiro, J., Antunes, S. C., Melo, A., Rocha, F., Flores, D., and Mansilha, C. (2024). Hydropedological characterization of a coal mining waste deposition area affected by self-burning. Hydrology, 11(5), 62. https://doi.org/10.3390/hydrology11050062

Gao, S., Li, J.S., Zhang, S. and Poon, C.S. (2025). A state-of-the-art review of solid waste leaching mechanisms and evaluation methodologies. Waste Management, 204, 114941. https://doi.org/10.1016/j.wasman.2024.114941

Garbacz, A., Nowak, A., Marzec-Grządziel, A., Przybyś, M., Gałązka, A., Jaroszuk-Ściseł, J., and Grzywaczewski, G. (2025). Impact of Coal Waste Rock on Biological and Physicochemical Properties of Soils with Different Agricultural Uses. *Sustainability*, *17*(6), 2603. https://doi.org/10.3390/su17062603

Godsey, S.E., Kirchner, J.W. and Clow, D.W. (2009). Concentration-discharge relationships reflect chemostatic characteristics of US catchments. Hydrological Processes, 23(13), 1844-1864. https://doi.org/10.1002/hyp.7315

Gromek, P. and Lowe, T. (2025). Ground robot technologies in wildfire risk reduction: the viewpoint of the fire service. Progress in Disaster Science, 20, 100435. https://doi.org/10.1016/j.pdisas.2025.100435

Hoxha, E., Symochko, L. and Pinheiro, M. N. C. (2025). The environmental impact of mining activities in Europe: a comprehensive analysis. EQA-International Journal of Environmental Quality, 66, 30-42.

International Energy Agency. (2025). Global Energy Review 2025. IEA. https://www.iea.org/reports/global-energy-review-2025

Karabyn, V. and Kochmar, I. (2025). Distribution of different forms of manganese in coal mining waste: A case study of the Vizeyska mine, Ukraine. IOP Conference Series: Earth and Environmental Science, 1499, 012045. https://doi.org/10.1088/1755-1315/1499/1/012045

Karabyn, V., Shuryhin, V., Shutiak, S., Chmiel, M. and Kulhanek, R. (2022). Strategic environmental assessment - underestimated tool for sustainable subsoil use. Environmental Problems, 7(3), 140-146. https://doi.org/10.23939/ep2022.03.140

Knapp, J.L. A., Li, L. and Musolff, A. (2024). Concentration-discharge relationships revisited: Overused but underutilised? Hydrological Processes. Advance online publication. https://doi.org/10.1002/hyp.15328

Kochmar, I. and Karabyn, V. (2023). Water extracts from waste rocks of the coal industry of Chervonohrad mining area (Ukraine): problems of environmental safety and civil protection. Ecological Engineering & Environmental Technology, 24(1), 247-255. https://doi.org/10.12912/27197050/156939

Kochmar, I., Karabyn, V. and Karabyn, O. (2022). Lead Speciation in the Technogenesis Zone of Coal Mining Sites (Case of Vizeyska Mine of Chervonohrad Mining Area, Lviv Region, Ukraine). Petroleum and Coal, 64(2): 445-454

Kochmar, I., Karabyn, V. and Kordan, V. (2024). Ecological and geochemical aspects of thermal effects on argillites of the Lviv-Volyn coal basin spoil tips. Scientific Bulletin of the National Mining University, 3, 100-107.

Kumar, R., Heße, F., Rao, P.S.C., Musolff, A. and Jawitz, J.W. (2020). Strong hydroclimatic controls on vulnerability to subsurface nitrate contamination across Europe. Nature Communications, 11, 6302. https://doi.org/10.1038/s41467-020-19955-8

Loboichenko, V. and Leonova, N. (2021). Assessment of the impact of natural and anthropogenic factors on the state of water objects in urbanized and non-urbanized areas in Lozova district (Ukraine). Ecological Engineering and Environmental Technology, 22(2), 69-76. https://doi.org/10.12912/27197050/135188

Long, P., Wang, G.-S., Zhang, S., Hu, S.-L. and Huang, Y. (2020). A mathematical model for column leaching of ion adsorption-type rare earth ores. International Journal of Minerals, Metallurgy and Materials, 27(4), 463-471. https://doi.org/10.1007/s12613-019-1883-9

Lousada, S., Delehan, S. and Khorolskyi, A. (2024). Application of dynamic programming models for improvement of technological approaches to combat negative water leakage in the underground space. Water, 16(14), 1952. https://doi.org/10.3390/w16141952

Martin, J., & Langman, J. B. (2024). Leachate experiments to evaluate weathering of waste rock for backfill aquifers in restored coal mine pits, Powder River Basin, USA. *Geosciences, 14*(1), 4. https://doi.org/10.3390/geosciences14010004

Merritt, P., & Power, C. (2022). Assessing the long-term evolution of mine water quality in abandoned underground mine workings using first-flush based models. *Science of the Total Environment, 846*, 157390. https://doi.org/10.1016/j.scitotenv.2022.157390

Monteiro, M., Santos, P., Espinha Marques, J., Flores, D., Azenha, M., & Ribeiro, J. A. (2025). Assessment of Potential Environmental Risks Posed by Soils of a Deactivated Coal Mining Area in Northern Portugal–Impact of Arsenic and Antimony. Pollutants, *5*(2), 15. https://doi.org/10.3390/pollutants5020015

Montgomery, D. C., Peck, E. A., & Vining, G. G. (2021). *Introduction to linear regression analysis* (6th ed.). Hoboken, NJ: Wiley.

Moroz, O.M., Hnatush, S.O. and Maslovska, O.D. (2020). Reduction of sulfur and oxidized forms of nitrogen by bacteria of Desulfuromonas sp., isolated from Yavorivske Lake, under the influence of ferrum citrate. Biosystems Diversity, 28(1), 78-85. https://doi.org/10.15421/012011

Mugova, E., Molaba, L., & Wolkersdorfer, C. (2024). Understanding the mechanisms and implications of the first flush in mine pools: Insights from field studies in Europe's deepest metal mine and analogue modelling. *Mine Water and the Environment, 43*, 73–86. https://link.springer.com/article/10.1007/s10230-024-00969-3

Orndorff, Z.W., Daniels, W.L., Zipper, C.E., Eick, M. and Beck, M. (2015). A column evaluation of Appalachian coal mine spoils' temporal leaching behaviour. Environmental Pollution, 204, 39-47. https://doi.org/10.1016/j.envpol.2015.03.049

Park, J.H., Li, X., Edraki, M., Baumgartl, T. and Kirsch, B. (2013). Geochemical assessments and classification of coal mine spoils for better understanding of potential salinity issues at closure. Environmental Science: Processes & Impacts, 15(6), 1235-1244. https://doi.org/10.1039/c3em30672k

Petlovanyi, M., Sai, K., Malashkevych, D., Popovych, V. and Khorolskyi, A. (2023). Influence of waste rock dump placement on the geomechanical state of underground mine workings. IOP Conference Series: Earth and Environmental Science, 1156, 012007. https://doi.org/10.1088/1755-1315/1156/1/012007

Proshad, R., Chandra, K., Islam, M., Khurram, D., Rahim, M.A., Asif, M.R. and Idris, A.M. (2025). Evaluation of machine learning models for accurate prediction of heavy metals in coal mining region soils in Bangladesh. Environmental Geochemistry and Health, 47(5), 1-25. https://doi.org/10.1007/s10653-024-01782-3

Rouhani, A., Newton, R.A., Al Souki, K.S., Quattrini, G. and Gusiatin, M.Z. (2024). A 6-year review status on soil pollution in coal mining areas from Europe. Environmental Geochemistry and Health, 46(10), 392. https://doi.org/10.1007/s10653-023-01666-7

Rouhani, A., Skousen, J. and Tack, F.M.G. (2023). An overview of soil pollution and remediation strategies in coal mining regions. Minerals, 13(8), 1064. https://doi.org/10.3390/min13081064

Skrobala, V., Popovych, V., Tyndyk, O. and Voloshchyshyn, A. (2022). Chemical pollution peculiarities of the Nadiya mine rock dumps in the Chervonohrad Mining District, Ukraine. Mining of Mineral Deposits, 16(4), 71-79. https://doi.org/10.33271/mining16.04.071

Stepova, K., Fediv, I., Mažeikiene, A., Šarko, J. and Mažeika, J. (2023). Adsorption of ammonium ions and phosphates on natural and modified clinoptilolite: Isotherm and breakthrough curve measurements. Water, 15, 1933. https://doi.org/10.3390/w15101933

Sutherland, C., Chittoo, B.S. and Samlal, A. (2023). The status of scientific development on the application of biosorption of heavy metals at laboratory and pilot-scale: A review. Desalination and Water Treatment, 299, 13-49. https://doi.org/10.5004/dwt.2023.29729

Tkachenko, H., Kurhaluk, N., Skaletska, N., Maksin, V. and Osadowski, Z. (2021). Elemental status and lipid peroxidation in the blood of children with endemic fluorosis. Biological Trace Element Research, 199(4), 1237-1245. https://doi.org/10.1007/s12011-020-02193-y

Tyndyk, O., Popovych, V., Sai, K., and Petlovanyi, M. (2024). Natural phytomelioration of the coastal water zone of man-made reservoirs in mining areas. E3S Web of Conferences, 526, 01005. https://doi.org/10.1051/e3sconf/202452601005

URL 1. https://meteopost.com. (accessed 1st August 2025).

Vladyko, O., Maltsev, D., Sala, D., Cichoń, D. and Buketov, V. (2022). Simulation of leaching processes of polymetallic ores using the similarity theorem. Rudarsko-Geološko-Naftni Zbornik, 37(5), 169-180.

Welch, C., Barbour, S. L. and Hendry, M. J. (2021). The geochemistry and hydrology of coal waste rock dumps: A systematic global review. Science of the Total Environment, 795, 148798.

Xu, K., Zhong, W., Qian, L., Xia, F., Han, X., Yu, X., & Zhu, X. (2025). Harnessing bio-modified coal gangue for mine wastewater remediation: a sustainable approach. Environmental Geochemistry and Health, 47(9). https://doi.org/10.1007/s10653-025-02698-0

Xu, W., Jin, Y., & Zeng, G. (2024). Introduction of heavy metals contamination in the water and soil: a review on source, toxicity and remediation methods. Green Chemistry Letters and Reviews, *17*(1). https://doi.org/10.1080/17518253.2024.2404235

SAŽETAK

Integrirano matematičko i fizičko modeliranje izluživanja ionskih soli iz rudarskoga otpada ugljena: implikacije za ekološku sigurnost i civilnu zaštitu

Odlagališta rudarskoga otpada iz eksploatacije ugljena predstavljaju znatan izvor otopljenih soli koje se mogu mobilizirati pod utjecajem oborina, što stvara rizike za ekološku sigurnost i sustave civilne zaštite. Ovo istraživanje usmjereno je na odlagalište jalovine Centralne flotacije Červonohrad u zapadnoj Ukrajini, gdje su ispitivani i termalno izmijenjeni i neizmijenjeni argiliti. Laboratorijska istraživanja izluživanja provedena su na uzorcima mase 100 g, koji su izluženi deioniziranom vodom radi simulacije procesa izluživanja pod kontroliranim uvjetima. Kumulativni volumeni procijeđene otopine iznosili su približno 432 L, što je omogućilo kvantifikaciju ukupnih otopljenih tvari te pojedinačnih ionskih doprinosa. Tijekom 24 sata provedeno je izluživanje kroz stupce brzinom od 300 $mL \cdot min^{-1}$ (ukupno 8,5 L recirkulirano, ≈ 432 L prošlo kroz uzorak), pri čemu je izmjerena konačna koncentracija ukupnih otopljenih tvari od 462 $mg \cdot L^{-1}$ za izgorjeli argilit i 185 $mg \cdot L^{-1}$ za neizgorjeli, dok su kumulativne mase izluženih soli iznosile 3,93 g odnosno 1,57 g (≈ 2,5 puta više za izgorjeli uzorak). Razlika u početnoj fazi izluživanja bila je još izraženija: nakon 2 sata (≈ 0,7 L) koncentracija je kod izgorjeloga uzorka iznosila 183 $mg \cdot L^{-1}$, a kod neizgorjeloga 50 $mg \cdot L^{-1}$ (≈ 3,7 puta više). Fizička opažanja povezana su s matematičkim modeliranjem radi uspostave odnosa između količine oborina i oslobađanja ukupnih otopljenih tvari. Rezultati upućuju na izraženu linearnu povezanost između godišnje količine oborina i oslobađanja soli iz procesa izluživanja, pri čemu termalno izmijenjeni materijali pokazuju znatno veće tokove iona. Ovaj integrirani modelni pristup pokazuje kako se laboratorijski podatci i jednostavni modeli mogu koristiti za predviđanje izluživanja onečišćujućih tvari, čime se pridonosi ekološkoj sigurnosti i planiranju mjera civilne zaštite u rudarskim područjima sklonim hidrološkim ekstremima.

Ključne riječi:
civilna zaštita, ekološka sigurnost, sustavi ranoga upozorenja, geokemija, prediktivno modeliranje, izluživanje

Author's contribution

Vasyl Karabyn (Dr Eng; Professor of Civil Protection): conceptualisation, methodology, supervision, writing - original draft, project administration. **Iryna Kochmar** (Lecturer): selected representative spoil materials, prepared the samples and carried out column experiments; she curated laboratory data and contributed to manuscript revision, mathematical modelling, writing - original draft. **Oksana Karabyn** (PhD; Associate Professor of Mathematics): formulation of the mathematical model, formal analysis; modelling, writing - original draft & editing. **Clint Sutherland** (Dr Eng; Associate Professor of Civil Engineering): methodology; supervision; writing - original draft & editing. **Valentyna Loboichenko** (Dr Eng; Professor of Civil Protection): methodology; supervision; writing - original draft & editing. **Andrii Khorolskyi** (PhD; Head of Laboratory): methodology; formal analysis; visualisation; writing - review & editing.
All authors have read and agreed to the published version of the manuscript.